ELSEVIER

Ultrasound in Med. & Biol., Vol. 23, No. 8, pp. 1171–1177, 1997

0301-5629/97 $17.00 + .00

PII S0301-5629(97)00125-7

● *Original Contribution*

DECAY CONSTANT OF DOPPLER FLOW WAVEFORM AS A POSSIBLE INDICATOR OF OVARIAN MALIGNANCY

RON TEPPER,* LAURENCE KESELBRENER,† MOSHE MANOR,* SHULAMIT EYAL,†
YORAM BEYTH,* YAIR ZIMMER† and SOLANGE AKSELROD†

*Department of Obstetrics and Gynecology, Sapir Medical Center, Kfar Saba, Israel; and †Abramson Center for Medical Physics, Tel-Aviv University, Tel Aviv 69978 Israel

(*Received* 30 *May* 1996; *in final form* 17 *June* 1997)

Abstract—The objectives of this study were to analyze the decay constant (τ) of the Doppler flow waveform in ovarian tumors; to determine if differences in this constant can discriminate between malignant and benign ovarian tumors; and to compare the decay constant to the known resistive index (RI), in order to determine its potential prognostic application. Patients with ovarian masses (46) were evaluated in a retrospective study; 13 had malignant tumors, 7 showed tumors with low malignant potential (LMP), 11 had benign masses, 4 had secondary ovarian metastases and 11 had functional ovarian masses. Doppler flow waves measured in the ovary before operation were analyzed from archival videotapes. The RI was calculated preoperatively, and the decay constant of the flow waveform was analyzed retrospectively. We approximated the decaying portion of the flow waveform from the systolic peak to the diastolic level to an exponential curve. Then, the decay constant associated with the flow signal was compared for different types of ovarian pathology. Ovaries with malignancies showed significantly higher mean values for the decay constant (89.7; 95% confidence interval 60.0–119.3) than those with benign tumors (41.8; 25.7–57.9) ($p < 0.007$), where τ is provided in pixels (in this study each pixel equals approximately 11.4 ms). The mean RI value for malignant tumors was 0.44 ± 0.12 whereas, in benign tumors, it was 0.622 ± 0.11. For the benign tumors, both τ and RI did not differ significantly from the measured indices in LMP tumors, metastases and functional ovarian findings. In addition, when the cutoff value of τ was set at 48, 92.3% of all malignancies were identifiable using only τ. This preliminary study indicates that the decay constant of the Doppler flow waveform is able to discriminate between malignant and benign masses and may, thus, provide substantial assistance as an additional parameter in the diagnosis of malignant ovarian tumors in postmenopausal patients. © 1997 World Federation for Ultrasound in Medicine & Biology.

Key Words: **Doppler flow waveform, Decay constant, Ovarian neoplasm.**

INTRODUCTION

Ovarian malignancies represent the primary cause of mortality due to gynecological cancer (Cramer 1986). To overcome the difficulty in distinguishing between benign and malignant ovarian findings, improved morphology-based classifications have been developed (Benacerraf et al. 1990; Herrman et al. 1987; Sassone et al. 1991). Such techniques somewhat enhance the predictive ability; nevertheless, in many cases, diagnostic uncertainty is still common.

Malignant tumors typically present increased angiogenesis (Folkman 1985) and, thus, display neovascularization. This results in lowered impedance in malignant ovarian tumors compared to that of benign ones (Kawai et al. 1992; Kurjak et al. 1992; Tepper et al. 1995; Weiner et al. 1992).

The Doppler flow technique offers a noninvasive, qualitative and quantitative measure of blood flow in the target organ. In recent years, it has increasingly been used to evaluate blood-flow resistance in the pelvic organs under different pathologic conditions. It provides more information in cases of adnexal torsion, malformation of pelvic blood vessels, myometrial perfusion for infertility investigations and, in cases of identification of pathologic waveforms, a means to distinguish between malignant and benign processes (Goswami et al. 1988; Shimamoto et al. 1987; Tepper et al. 1994, 1995, 1996). The ultrasound Doppler waveform is used to obtain an indirect indication of resistance. Although the values of computed resistance to flow have been found to correlate

Address for correspondence: Solange Akselrod, Ph.D., Medical Physics Department, School of Physics and Astronomy, Tel Aviv University, Tel Aviv 69978 Israel.

with the degree of neovascularization in various gynecological tumors (Taylor et al. 1988; Tepper et al. 1995), in many cases the information may not be adequate to establish the desired differentiation (Bourne et al. 1989; Bromley et al. 1994; Tepper et al. 1995; Valentin et al. 1994). The diagnostic power is enhanced by the combination of functional information (supplied by the Doppler technique) and morphological data (from B-scan ultrasonography).

The objective of the present study was to estimate the decay constant of the flow waveform in ovarian tumors, based on the delineation of the postsystolic decay curve, and to investigate its ability to characterize the tumor. We, thus, strove to obtain an additional functional parameter to improve the discrimination between benign and malignant findings in the ovary.

MATERIALS AND METHODS

The Doppler flow waveforms in ovarian tissue were evaluated retrospectively in a group of 46 women, aged from 27 to 79 y, in the ultrasound unit of our gynecology department. Inclusion criteria for the study group were as follows: the maximum period for performance of the Doppler test on the women was 4 days prior to ovary excision; all tumors were examined histologically according to the World Health Organization classifications. Complete histological data on the excised ovaries was available, and video documentation of the examination was available, permitting retrospective investigation of the blood flow in the ovarian tissue.

The women were divided retrospectively into 5 histological groups: Group A: 13 women with malignant ovarian findings and mean age of 54 ± 12.7 y; 8 women were postmenopausal, 6 were in stage 1 and 7 in stage 3 of the disease. Group B: 14 women with benign ovarian findings and mean age of 62.7 ± 15.7 y; 9 women were postmenopausal. Group C: 7 premenopausal women with low malignant potential (LMP) ovarian findings; mean age was 38.7 ± 5.1 y; all were in stage 1 of the disease. Group D: 4 women with secondary ovarian metastases; mean age was 58.5 ± 6.6 y. Group E: 8 premenopausal women with functional ovarian findings; mean age was 40.0 ± 7.3 y.

Patients were scanned transvaginally using an Aloka SSD 680 (Aloka Co. Ltd., Tokyo, Japan) with a 5-MHz transvaginal probe. Pulse repetition frequencies were 1–25 kHz, and the gate width 1 mm. Wall filters were set at a minimal 50 Hz. Spatial peak temporal average intensity was less than 80 mW/cm^2. Color-flow Doppler arterial waveform studies were performed to identify several areas of blood flow within the tumor or on its margins. The value of the resistive index (RI) was calculated from the envelope of the Doppler shift frequencies. The RI was defined as the ratio of the difference between the frequencies at peak systole and end diastole to the frequency at systole. The representative value used for the mean RI was obtained by averaging its values for 3 consecutive waveforms with the lowest RI.

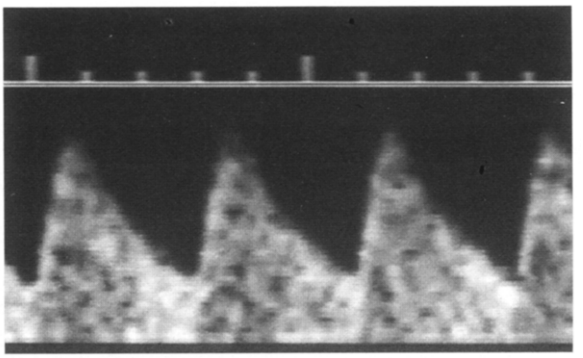

Fig. 1. Image of Doppler spectral waveform from ovarian tumor (before image processing). Positive flow is upward. The image was magnified for display.

WAVEFORM DELINEATION AND COMPUTATION OF DECAY CONSTANT

Waveform delineation

The technique for waveform delimitation was based on brightness differentiation of the pixels comprising the Doppler flow picture. Automatic flow waveform detection was achieved by simple mathematical manipulation of the pixel grey levels, as described below. Our aim was to approximate automatically as closely as possible the typical flow waveform obtained manually by a skilled clinician during an examination. The technique consisted of 3 phases:

Image grabbing. The flow waveform patterns were selected from the video recordings and sampled into an IBM-compatible PC, using a DT2851 frame-grabber (Data Translation, Inc., Marlboro, MA, USA), achieving a resolution of 512 × 512 pixels and 256 gray levels. Sampling was performed while freezing the image on the videoplayer. An example of the obtained waveform is provided in Fig. 1.

Image smoothing. After sampling, the image was smoothed by a square median filter, to remove noise in the region of the Doppler signals and to facilitate detection of its borders. The median, a nonlinear filter, was found to be more suitable than any linear low-pass filter, because it removed noise but still preserved the sharp edges of the Doppler signals. This edge was actually the flow waveform that we sought to delineate.

Waveform detection algorithm. To obtain the shape of the flow curve, we designed an algorithm to detect the

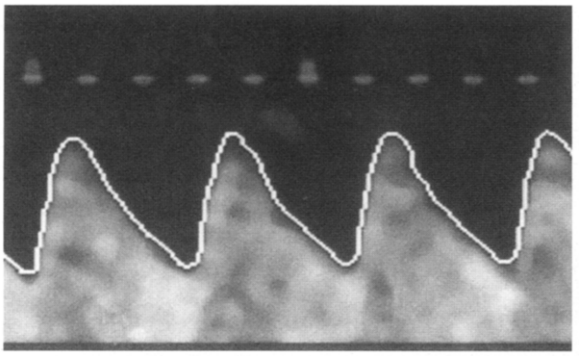

Fig. 2. Result of automatic processing of waveform from Fig. 1, after smoothing and edge detection. The white curve is the waveform *W(t)*. Next, exponential decay curve is fitted to the postsystolic decay of the flow wave. The image was magnified for display.

upper frequency observed or the *y*-coordinate of the flow curve (the *x*-coordinate was simply time). First, the user was required to point out the baseline level of Doppler signals (zero flow). Then, the user selected the region-of-interest (ROI) in the bright region for which border detection was to be made.

The basic approach of the detection algorithm was to identify the region of Doppler waveform signals as a bright continuous region on a dark background. Then, automatically, the algorithm scanned vertically from baseline, searching the end of the bright region (*y*-coordinate) in column after column (for every *x*-coordinate). The smoothing procedure previously performed on the image enabled adequate detection of the transition from bright to dark. After subtracting the *y*-coordinate of the baseline level from the *y*-coordinate of the transition, we obtained the waveform *W(t)* of the flow signal as a function of time (see Fig. 2). This difference was then saved as an ASCII file, to be used as the input for computation of the exponential decay.

To evaluate the automatically processed waveform *W(t)* and to assess its deviation from the original (manually determined) value described in the presurgical examination, the RI parameter was automatically computed. This allowed us to estimate the degree of correspondence between the original and the computed parameters. To compute RI, the same criteria were applied as during a manual evaluation performed in the initial examination, that is, by computing the maximum and minimum values along the boundary line and calculating the ratio between these amplitudes.

Calculating the decay constant

After finding the *W(t)* curve, which digitally describes the flow, a number of waves with the lowest RIs were selected for each subject to perform the computation of the waveform decay constant. This constant is a mathematical parameter reflecting the rate of postsystolic decay of the flow wave. The decay constant was calculated by approximating the obtained waveform to an exponential curve according to the following expression:

$$\tilde{W}(t) = Ke^{-t/\tau} + C \qquad (1)$$

where τ = the postsystolic waveform decay constant, C = the constant to which the waveform tends at infinity ($C = 0$, assuming the curve tends toward zero), t = time from systolic peak, and K = a mathematical constant describing initial flow level.

Several attempts were made to calculate the decay constant (τ) in terms of the parameters, such as various values of the C constant, or various parts of the diastolic decay curve. The most reproducible results were obtained for $C = 0$ and using the entire diastolic curve (from peak systole to end diastole) to calculate the decay constant.

Figure 3a, b, c presents the results obtained for the 3 waves shown in Fig. 2. For each wave, + represents the detected flow waveform [the curve *W(t)*] and · provides the exponential curve formed using the obtained value of τ for the wave [the curve $\tilde{W}(t)$]. The values of τ computed for the leftmost, middle and rightmost waves in Fig. 2 (related to Fig. 3a, b and c, respectively) are 37.5, 37.9 and 39.7, respectively. These values of τ are provided in pixels where, for this study, each pixel equals approximately 11.4 ms (88 pixels equal 1 s). This time-scale is illustrated by the ruler at the top part of Figs. 1 and 2, where the distance between 2 large marks on this ruler represents 1 s.

DATA ANALYSIS

Of 46 patients retrospectively evaluated in the study, 21 (45.6%) were postmenopausal. The evaluations entailed color-flow images and histologic analysis of the pelvic mass. Pathologically, there were 13 malignant (Group A), 14 benign (Group B), 7 LMP (Group C), 4 metastastic (Group D) and 8 functional ovarian (Group E) tumors.

Postoperatively, off-line, each image was grabbed as a still frame from the videotape. The above algorithm was applied for waveform delineation, and a continuous waveform *W(t)* was plotted automatically. Then, the algorithm automatically performed 2 independent procedures: fitting the flow waveform *W(t)* to an exponential curve $\tilde{W}(t)$, thus obtaining τ, and computing an automatic evaluation of RI, from the fitted waveform $\tilde{W}(t)$. This automatically obtained RI value was compared with the original RI value manually obtained preoperatively by RT.

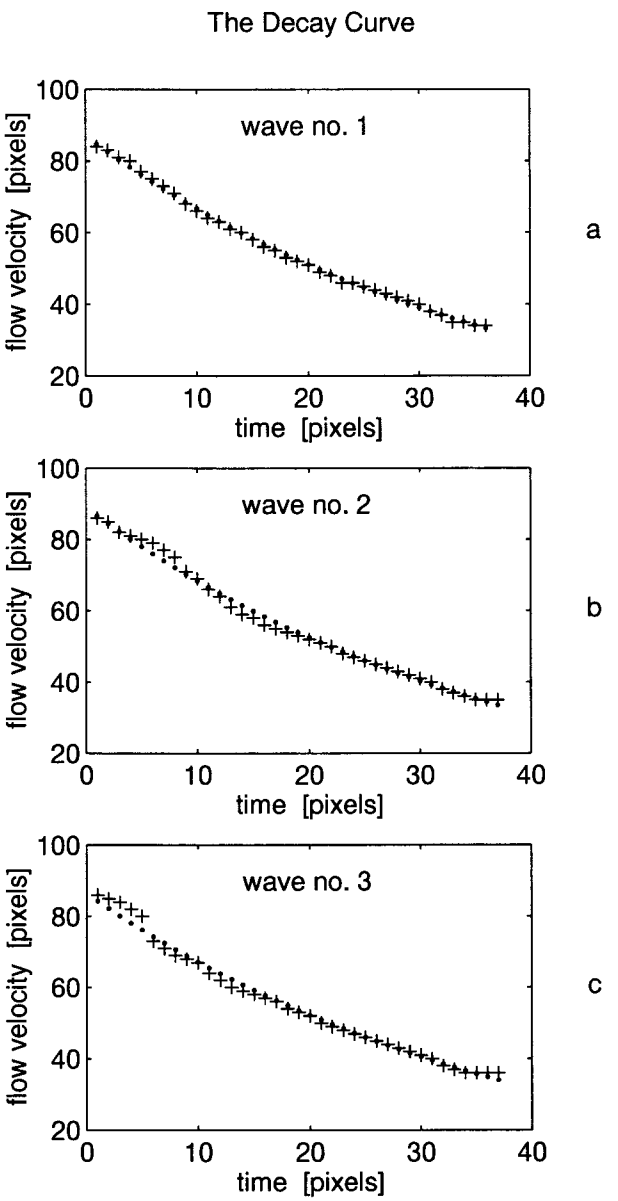

Fig. 3. The exponential fit for the 3 waves shown in Fig. 2. For each wave, + represents the detected flow waveform [the curve $W(t)$] and · provides the exponential curve formed using the obtained value of τ for the wave [the curve $\tilde{W}(t)$]. In Fig. 3, a, b and c correspond to the leftmost, middle and rightmost waves in Figs. 1 and 2, respectively.

The positive and negative predictive values for the patients were determined on the basis of both parameters extracted from the Doppler flow curve, namely the decay constant τ and RI.

RESULTS

The automatically computed RI value was compared to the initial RI value measured manually by one examiner (RT) prior to surgery. The manually computed (MC) RI values and computer-calculated (CC) RI values, listed by morphological type, are presented in Table 1. A high degree of correlation ($r = 0.925$) and no significant difference in the mean values were found between the manually calculated RI values and those calculated automatically after the waveform processing.

In this study, an automatic exponential fit was computed to the blood-flow curve, assuming the constant C to be zero. To assess the validity of τ according to its estimate obtained from a single wave, we tested its reproducibility in a subgroup of 31 subjects by using a number of successive waves originating from the same ovary in each of these cases. An excellent agreement was found between the τ measurement obtained for the various waves for the same individual. The standard deviation σ_τ observed between the various τ values for each individual ranged from 0.32 to 5.3 (on the average, σ_τ was 2.75) for this test group of subjects, in which τ ranged from 35 to 70. We therefore assumed that τ obtained from a single randomly chosen wave, was a reliable representative of the decay rate of the remaining waveforms measured in the same ovary and, thus, performed our analysis on the patient groups described.

The τ and RI evaluations were performed separately for the malignant and benign tumor groups, by treating each wave as described above. The results of the Doppler flow waveform indices are shown in Tables 2 and 3; significant pairwise differences are indicated by asterisks. The mean τ obtained for the malignant group (Group A [A1 to A3], 89.7 ± 49.0) was significantly greater ($p < 0.007$) than that calculated for the group with benign histology (Group B [B1 to B5], 41.8 ± 24.0), but not significantly different from the LMP group or those with secondary ovarian metastases (Groups C, D or E [E1 to E2]).

In addition, the correlation between the decay constant values and the surgical stage was assessed. In 6 women at Stage 1 (different histology), the mean value for τ was 60.83 (± 26.7) compared to a mean value of 102.2 (± 49.5) in 8 women in Stage 3 of the disease (7 with similar histology). A tendency towards increased τ was observed among women in more advanced malignant stages, but the difference was not significant.

The correlations between RI values and τ were examined in the different pathologic groups (Table 2). Pearson's correlation between τ and RI values in the malignant group was not significant ($r = -0.33$). There was also a lack of correlation between these parameters in the benign group ($r = -0.459$).

When τ was assessed only in postmenopausal patients and its cutoff value set at 48, PPV was 100% and NPV 57%. For the combined pre- and postmenopausal group (A), when τ's cutoff value was set at 48, the

Table 1. Manually computed (MC) vs. computer computed (CC) resistive indices for 4 different tumoral histologic groups

	Group A malignant (n = 13)		Group B benign (n = 14)		Group C LMP (n = 7)		Group D metastastic (n = 4)	
	RI-MC	RI-CC	RI-MC	RI-CC	RI-MC	RI-CC	RI-MC	RI-CC
Mean	0.438	0.382	0.579	0.535	0.508	0.496	0.52	0.478
± SD	0.117	0.135	0.112	0.139	0.06	0.07	0.09	0.123
95% CI	0.376–0.409	0.31–0.453	0.53–0.63	0.474–0.597	0.441–0.568	0.421–0.571	0.349–0.691	0.25–0.70

CI = confidence interval; RI = resistive index.

positive predictive value (PPV) was 80.7% and the negative predictive value (NPV) was 47.4%.

When discriminating according to RI for the detection of ovarian pathology in postmenopausal patients, PPV was found to be 75% and NPV 40% when considering the cutoff RI value of 0.47. This RI cutoff of 0.47 was chosen because, based on previous experience, this value represents the border value best differentiating between benign and malignant ovarian tumors, with an 88% malignancy detection rate and a 14% false-positive rate (Tepper et al. 1995).

DISCUSSION

Adopting Folkman's theory, the angiogenosis appearing in the hyperplastic cells acts as a preliminary marker of neoplastic transformation (Folkman et al. 1989). In contrast to healthy tissue, neovascularization in tumoral mass continues as long as there is angiogenic induction. In animal experiments (Folkman 1985; Folkman and Kalgsbrun 1987), tumor genesis has been shown to be affected by angiogenic inhibitors.

The systolic peak of the flow waveform is a function of cardiac contraction, whereas diastolic flow depends mainly on vascular peripheral resistance (Thompson et al. 1988). It can, therefore, be assumed that flow between systole and diastole is strongly affected by peripheral resistance specific to the investigated tissue. This is true for some, but not for all, malignant tumors where neovascularization lowers the resistance to flow, and a higher end-diastolic flow is recorded, thus causing a slower postsystolic waveform decay compared with waveform decay in healthy tissue.

Currently, the relationship between systolic and diastolic flow levels is expressed by generally accepted formulas to assess the resistance (PI, RI), whereas the rate of postsystolic waveform decay has not yet been assessed. However, a significant overlap has been observed between the flow characteristics of benign and malignant ovarian tumors when described by PI and RI (Hamper et al. 1993; Tekay and Joupilla 1992).

In this study, we developed a computerized approach that can be used to analyze the flow waveform and compute its decay constant. We tested whether or not our computer-defined curve fits the original curve, and found good agreement between the RI values measured manually during the clinical examination and those computed automatically from the curve fitted to the recorded Doppler flow images. We may, therefore, conclude that the image processing and line search were performed in a way such that the fitted waveform obtained after processing is a good representation of the original examination curve, normally drawn by the physician.

Table 2. Comparison of Doppler waveform examinations by ovarian pathology

	Group A malignant (n = 13)	Group B benign (n = 14)	Group C LMP (n = 7)	Group D metastastic (n = 4)	Group E functional (n = 8)
τ					
mean	89.7†	41.8†	54.4	56	67.2
95% CI	60–119.3	25.7–57.9	34.5–73.4	–	43.7–90.7
RI					
mean	0.45†	0.62†	0.51	0.52	0.52
95% CI	0.37–0.52	0.54–0.69	0.45–0.57	0.35–0.69	0.46–0.58

CI = confidence interval; RI = resistive index; τ = decay constant; † significant difference ($p < 0.05$) between benign (Group B) and malignant tumors (Group A).

Table 3. Intraovarian waveform decay (τ) in ovarian masses arranged by histologic diagnosis.

Group	Diagnosis	n	τ Mean	τ ± SD	95% Coefficient interval
A1	Serous adenocarcinoma	9	103.5	51	64.1–143
A2	Undifferentiated Ca	2	41.3	25	
A3	Endometrial Ca	2	75.8	20	
B1	Inclusion cyst	4	25.7‡	16	0.8–51
B2	Serous cystadenoma	4	48.8	17	21.1–76.4
B3	Fibrothecoma	1	82.7		
B4	Adenofibroma	2	51.4	34	
B5	Endomedrioid	3	40.97	23	
C1	Mucinous and serous cystadenoma (LMP)	7	54.37†	21	34.5–74.3
D1	Metastases to ovary	4	55.4	44	
E1	Hemorrhagic cyst	3	85.5	37	63.5–107.5
E2	Follicular cyst	5	72.0	35	27.6–116.3

† Significant difference ($p < 0.03$) between A_1 and C_1; ‡ Significant difference ($p < 0.012$) between A_1 and B_1.

As commonly practiced when computing flow resistance, the average of 3 waves is taken as a representative index of flow resistance in the trace recorded. We found that the decay constant of successive waves was highly consistent. This supports the validity of accepting a single-wave decay constant as representative of a series of postsystolic decay curves, as further applied in this study.

The decay constant was significantly higher (mean 89.7, 95% confidence interval (CI) 60–119.3) in the group with malignant ovarian tumors (Group A) than in the group of benign tumors (Group B) (mean 41.8, 95% CI 25.7–57.9; $p < 0.007$). This did not apply to LMP tumors (Group C) or to ovarian metastases (Group E).

As a single index representing the contribution of the flow processed for the identification of a malignant finding, independent of the examinee's age, $\tau > 48$ showed higher sensitivity and specificity than RI < 0.47. The low correlation value between RI and τ computed on the same wave ($r = -0.33$) suggests a degree of independence between these parameters. Thus, not only the relationship between systolic and diastolic flow (RI), but also the mode of decay (τ), provides information useful for the interpretation of the ovarian flow waveform.

Our results seem to indicate that diastolic flow in malignant tissue will be higher, with slower postsystolic flow waveform decay and larger τ than in benign tissue flow, as a function of the extent of neovascularization. We estimate that the rate at which the flow decays to its diastolic level (*i.e.*, the decay constant) may be of highly predictive value in postmenopausal ovaries (sensitivity = 80%, specificity = 100%). Due to the overlap in τ for premenopausal malignant tumors (τ 89.7; 95% CI 60–119.3) and premenopausal benign functional tumors (Group E) (τ 67.2; 95% CI 43.7–90.7), we chose to evaluate τ in the postmenopausal group, because individuals in this group are not expected to display neovascular alterations of physiological origin, such as ovulation or luteal process.

Our results indicate that this additional method of analyzing the Doppler flow waveform contributes valid clinical information for the differential diagnosis of ovarian tumors. Further investigation is warranted in ovarian and other neoplasms to establish the diagnostic significance of τ as an acceptable index, in addition to the established RI and PI indices, and to identify which combination of these indices would yield optimal results in ovarian diagnoses.

Acknowledgements—The authors thank Sally Esakov for technical assistance, and the Abramson Research Fund of the Tel Aviv University for their support.

REFERENCES

Benacerraf BR, Finkler NJ, Wojciechowski C, Knapp RC. Sonographic accuracy in the diagnosis of ovarian masses. J Reprod Med 1990; 35:491–495.

Bourne T, Campbell S, Steer C, Whitehead MI, Collins WP. Transvaginal color flow imaging: a possible new screening technique for ovarian cancer. Br Med J 1989;299:1367–1370.

Bromley B, Goodman H, Banacerraf B. Comparison between sonographic morphology and Doppler waveform for the diagnosis of ovarian malignancy. Obstet Gynecol 1994;83:434–437.

Cramer DW. Epidemiologic and statistical aspects of gynecologic oncology. In: Knapp RC, Berkowitz RS, eds. Gynecologic oncology. New York: Macmillan, 1986:201–222.

Folkman J. Tumor angiogenesis. Adv Cancer Res 1985;43:175–203.

Folkman J, Kalgsbrun M. Angiogenic factors. Science 1987;235:442–427.

Folkman J, Watson K, Ingber D, Hanahan D. Induction of angiogenesis during the transition from hyperplasia to neoplasia. Nature 1989; 339:58–61.

Goswami RK, Williams G, Steptoe PC. Decreased uterine perfusion: a cause of infertility. Hum Reprod 1988;3:955–959.

Hamper UM, Sheth S, Abbas FM, Rosenshein NB, Aronson D, Kurman RJ. Transvaginal color Doppler sonography of adnexal masses: differences in blood flow impedance in benign and malignant lesions. AJR 1993;160:1225–1228.

Herrman UJ, Gotfried WL, Goldhirsch A. Sonographic patterns of

ovarian tumors: prediction of malignancy. Obstet Gynecol 1987; 77:777–781.

Kawai M, Kano T, Kikkawi F, Maeda O, Oguchi H, Tomada Y. Transvaginal Doppler ultrasound with color flow imaging in the diagnosis of ovarian cancer. Obstet Gynecol 1992;79:163–167.

Kurjak A, Schulman H, Sosic A, Zalud I, Shalan H. Transvaginal ultrasound, color flow and Doppler waveform of the postmenopausal adnexal mass. Obstet Gynecol 1992;80:917–921.

Sassone AM, Timor-Tritsch IE, Artner A, Westhoff C, Warren WB. Transvaginal sonographic characterization of ovarian disease: a new scoring system to predict ovarian malignancy. Obstet Gynecol 1991;78:70–76.

Shimamoto K, Sukuma S, Ishigaki T, Makino N. Intratumoral blood flow: evaluation with color Doppler echography. Radiology 1987; 165:683–685.

Taylor KJW, Ramos I, Carter D, Morse SS, Snower D, Fortune K. Correlation of Doppler ultrasound tumor signals with neovascular morphologic features. Radiology 1988;166:57–62.

Tekay A, Joupilla P. Validity of pulsatility and resistance indices in classification of adnexal tumors with transvaginal color Doppler ultrasound. Ultrasound Obstet Gynecol 1992;2:338–344.

Tepper R, Altaras M, Goldberger S, Zalel Y, Cordoba M, Beyth Y. Color Doppler ultrasonographic findings in low and high grade endometrial stromal sarcomas. J Ultrasound Med 1994;13:817–819.

Tepper R, Lerner-Geva L, Altaras M, Goldberger S, Ben-Baruch G, Markov S, Cohen I, Beyth Y. Transvaginal color flow imaging in the diagnosis of ovarian tumors. J Ultrasound Med 1995;14:731–734.

Tepper R, Zalel Y, Altaras M, Ben-Baruch G, Beyth Y. Transvaginal color Doppler ultrasound in the assessment of invasive cervical carcinoma. Gynecol Oncol 1996;60:26–29.

Thompson RS, Trudinger BJ, Cook CM. Doppler ultrasound waveform indices: A/B ratio, pulsatility index and Pourcelot ratio. Br J Obstet Gynaecol 1988;95:581–588.

Valentin L, Sladkevicius P, Marsal K. Limited contribution of Doppler velocimetry to differential diagnosis of extrauterine pelvic tumors. Obstet Gynecol 1994;83:425–433.

Weiner Z, Thaler I, Beck D, Rottem S, Deutsch M, Brandes JM. Differentiating malignant from benign ovarian tumors with transvaginal color flow imaging. Obstet Gynecol 1992;79:159–162.